



Research articles

Tilted magnetisation for domain wall pinning in racetrack memory

Tianli Jin^{a,1}, Funan Tan^{a,1}, Calvin Ching Ian Ang^a, Weiliang Gan^a, Jiangwei Cao^b,
Wen Siang Lew^{a,*}, S.N. Piramanayagam^{a,*}

^a School of Physical and Mathematical Sciences, Nanyang Technological University, 21, Nanyang Link, Singapore 637371, Singapore

^b Key Laboratory for Magnetism and Magnetic Materials of the Ministry of Education, Lanzhou University, Lanzhou 730000, People's Republic of China

A B S T R A C T

The interest in spintronics devices based on domain wall (DW) motion has gained attention for many years. However, the stochastic behaviour of DW motion is still a fundamental issue for the practical implementation of DW devices. In this study, we demonstrate that effective domain wall pinning can be achieved by using exchange interaction between Co/Ni multilayer with perpendicular magnetic anisotropy (PMA) and Co layer with in-plane magnetic anisotropy (IMA) to create locally tilted magnetisation. The strength of exchange interaction is tuned by varying the thickness of spacer layer Pt between the PMA and IMA layers, thus forming different tilt angles. Micromagnetic simulations were performed to verify the relation between pinning field and magnetisation tilt angle. Polar Kerr microscopy shows the current-driven DW pinning and depinning in the Co/Ni multilayer device with Co crossbars, where the thickness of spacer layer Pt is 1 nm. The proposed approach can potentially be used in future DW memory device applications.

1. Introduction

Spintronic devices based on domain wall (DW) motion has garnered the curiosity of researchers working on it due to its potential applications [1–5]. The three-dimensional domain wall memory combines the advantages of hard disk drive (HDD), such as high capacity [3,6], and magnetic random-access memory (MRAM) [7–10], such as low energy consumption and ultrafast operation. High capacity can be achieved by arranging a series of ferromagnetic nanowires on a wafer with vertical or horizontal configurations. For reading purpose, each nanowire is assembled with a tunnel magnetoresistance (TMR) sensor. DWs are driven to the TMR sensors along the wire for reading. Since there is no mechanical motion in DW memory's reading and writing processes, it is expected to be more energy efficient. Pulsed spin current with a duration of nanoseconds and an amplitude of 10^{10} A/m² [11–14], was reported to drive DWs, up to high speeds of kilometre per second [15].

DW motion shows stochastic behaviour in the presence of magnetic field and electric current [16–18]. The critical challenge for DW memory application is the control of DW position at the nanoscale regime. In previous studies, many groups have reported that the creation of notches along the wire is a successful method for DW pinning by creating an energy potential [19–21]. However, notch fabrication requires high-resolution lithographic technology. More importantly, it is not uniform due to the various notch size from process variation. We have studied metal diffusion and ion-implantation to tune magnetic properties locally to pin DWs [22,23]. Those non-geometrical methods

have been shown to be useful to control DW motion precisely. However, metal diffusion requires high-temperature annealing, which destroys the perpendicular magnetic anisotropy (PMA) for multilayer samples. In this letter, we propose an alternative approach to the formation of pinning sites using locally tilted magnetisation and explore the physics and device characteristics.

2. Micromagnetic simulation

At first, we performed micromagnetic simulation using mumax3 to demonstrate that a tilted magnetisation can pin DW in PMA nanowire [24]. The model is shown in Fig. 1(a). The nanowire with PMA carries data bits based on the out-of-plane magnetisation direction. By depositing an in-plane magnetic anisotropic (IMA) layer at desired positions, the magnetisation of the PMA nanowire is tilted locally, and this region acts as a pinning site to control domain wall motion. The PMA nanowire was set with a dimension of 1024 nm in length, 144 nm in width and 2 nm in thickness. The parameters used are: the magnetic anisotropy $K_0 = 8 \times 10^5$ J/m³, the saturation magnetisation $M_{s0} = 6 \times 10^5$ A/m, the damping constant $\alpha = 0.1$ and the exchange stiffness $A_0 = 13 \times 10^{-12}$ J/m [25]. In certain cases, the damping constant α was varied to study its effect. The magnetisation direction is initialised to a saturated state along z -direction (0,0,1).

Firstly, we studied the DW dynamics in PMA nanowire without tilted magnetisation. The DW dynamics under applying magnetic field were described by the Landau–Lifshitz–Gilbert (LLG) equation,

* Corresponding authors.

E-mail addresses: WenSiang@ntu.edu.sg (W.S. Lew), prem@ntu.edu.sg (S.N. Piramanayagam).

¹ These authors contributed equally to this work.

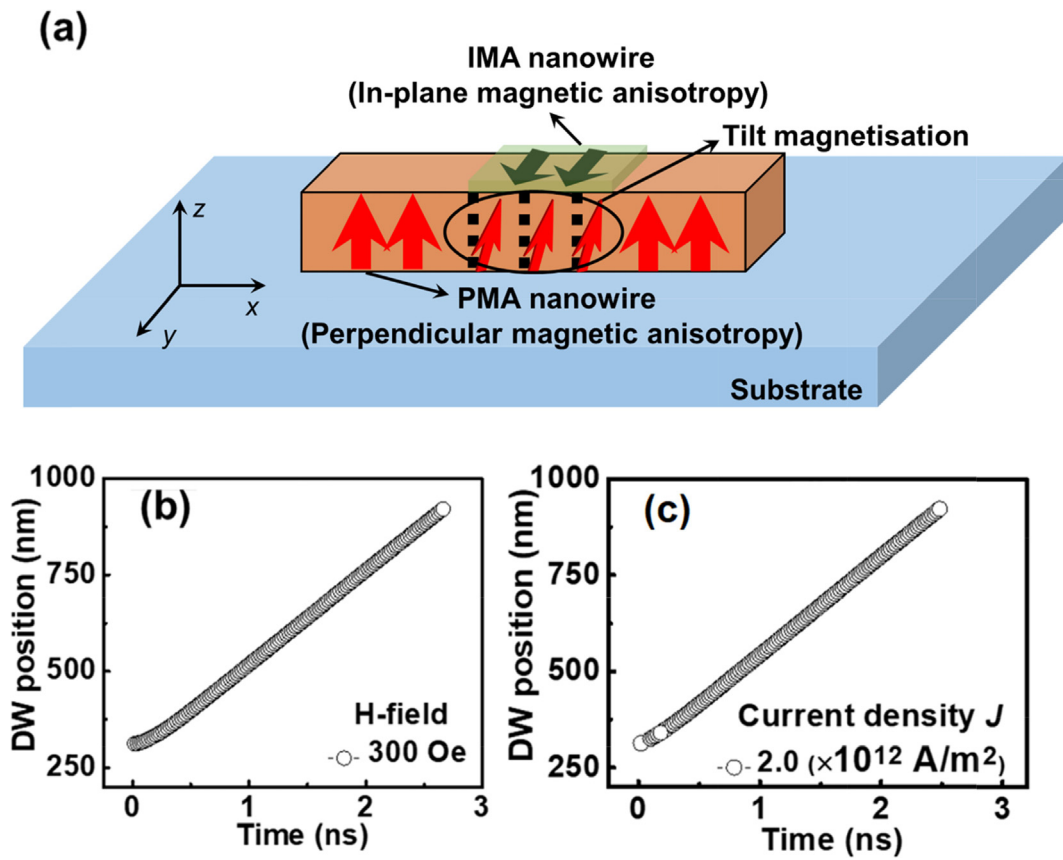


Fig. 1. (a) The simulation model built in this study. The nanowire along x direction displays perpendicular magnetic anisotropy (PMA) and the magnetisation is tilted by an in-plane magnetic anisotropic (IMA) nanowire. DW position vs. time driven by (b) magnetic field and (c) current. DW velocities are 240 m/s and 254 m/s for the magnetic field driven and current driven DWs respectively.

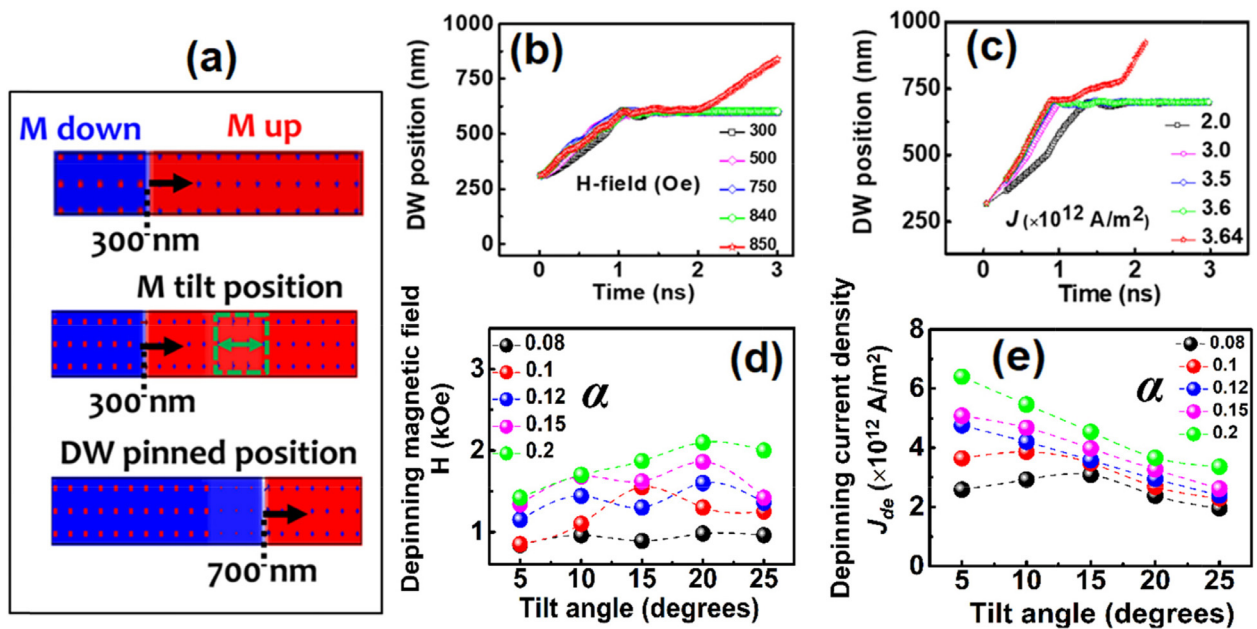


Fig. 2. (a) The schematic of DW pinning at tilted magnetisation position. The DW position in PMA nanowire with tilted magnetisation pinning site against time driven by different (b) magnetic fields and (c) electric currents. Depinning (d) magnetic field and (e) electric current density at different angles and values of damping constant α .

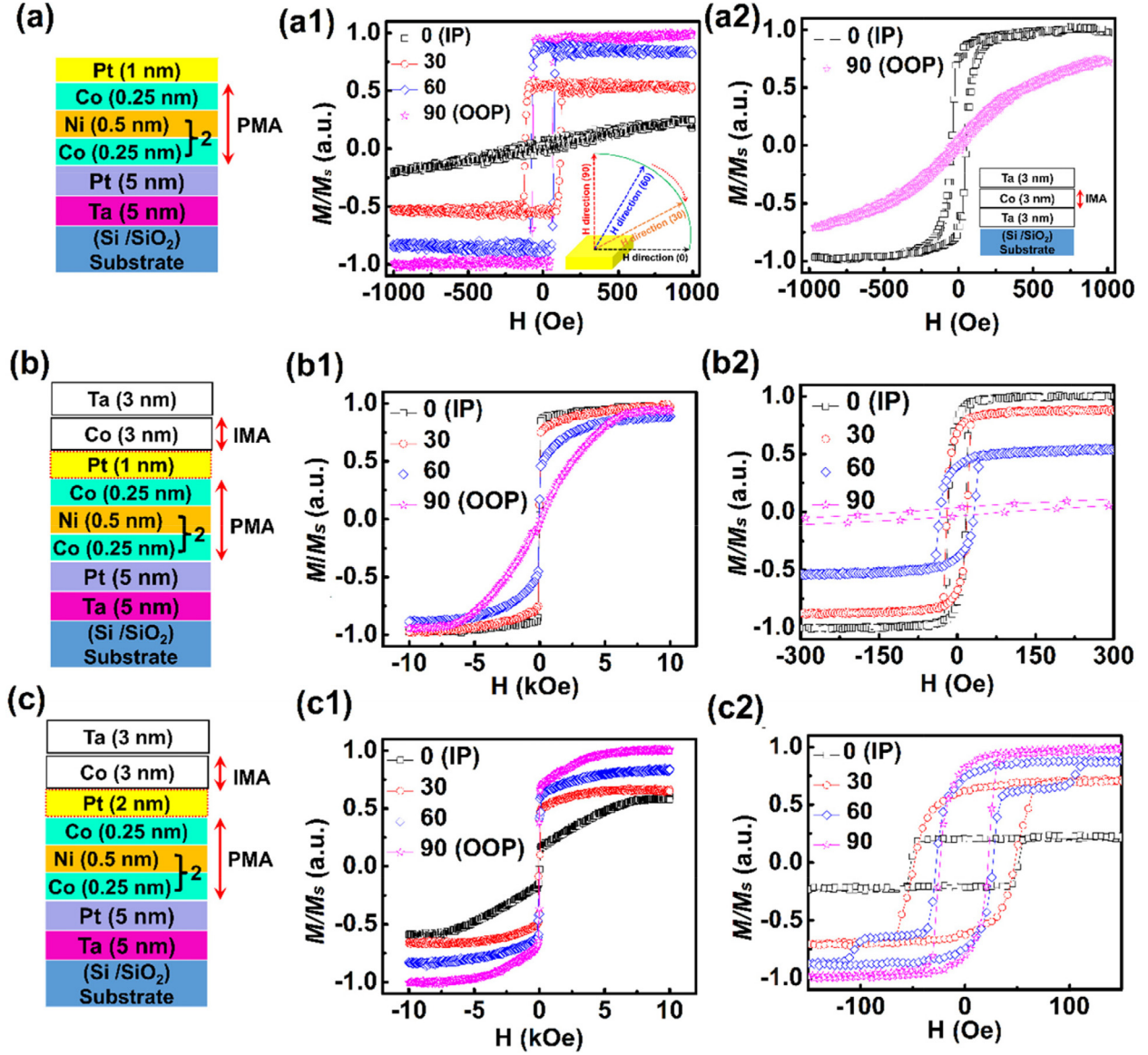


Fig. 3. (a) The stack of (Co/Ni)₂ PMA multilayer. (a1) and (a2) The hysteresis loops for (Co/Ni)₂ PMA and Co IMA samples at different directions. The inset in (a1) is the schematic of applied magnetic field (H) direction. The angle represents the angle between applied magnetic field and the film-plane. The inset in (a2) is the Co IMA stack. (b) and (c) The diagram of (Co/Ni)₂ multilayer with IMA Co layer, and the spacer layer Pt between them is 1 nm and 2 nm respectively. (b1) and (b2) The hysteresis loops for (Co/Ni)₂ multilayer sample with IMA Co layer along different directions, where the spacer layer Pt is 1 nm. (c1) and (c2) The hysteresis loops for (Co/Ni)₂ multilayer sample with IMA Co layer along different directions, where the spacer layer Pt is 2 nm. Images (b2) and (c2) are the zoom-in images of (b1) and (c1).

$$\frac{\partial \mathbf{M}}{\partial t} = -\frac{\gamma}{1 + \alpha^2} (\mathbf{M} \times \mathbf{H}_{eff}) - \frac{\gamma \alpha}{1 + \alpha^2} (\mathbf{M} \times (\mathbf{M} \times \mathbf{H}_{eff}))$$

where γ is the gyromagnetic ratio, α is the Gilbert damping constant, \mathbf{M} is the magnetisation, and the \mathbf{H}_{eff} is the effective field acting on the local magnetic moment \mathbf{M} which includes the external field, perpendicular anisotropy, exchange interaction and magnetostatic interaction. When the current was sent to the system, the additional torque, named as spin-transfer torque according to Zhang and Li [26], will act on the magnetisation. The DW dynamics were described by the extended LLG equation by taking into account both the adiabatic and non-adiabatic spin-transfer torques,

$$\begin{aligned} \frac{\partial \mathbf{M}}{\partial t} &= -\frac{\gamma}{1 + \alpha^2} (\mathbf{M} \times \mathbf{H}_{eff}) - \frac{\gamma \alpha}{1 + \alpha^2} (\mathbf{M} \times (\mathbf{M} \times \mathbf{H}_{eff})) \\ &\quad - \frac{\xi \alpha + 1}{1 + \alpha^2} \mathbf{M} \times (\mathbf{M} \times (\mathbf{u} \cdot \nabla) \mathbf{M}) - \frac{\xi - \alpha}{1 + \alpha^2} (\mathbf{M} \times (\mathbf{u} \cdot \nabla) \mathbf{M}) \end{aligned}$$

where ξ is the degree of non-adiabatic, which we set $\xi = 0.3$. The parameter \mathbf{u} has the units of velocity, which is proportional to current density \mathbf{j} and can be expressed as,

$$\mathbf{u} = \frac{\mu_B}{2e\gamma M_s (1 + \xi^2)} \mathbf{j}$$

where μ_B is the Bohr magneton and M_s the saturation magnetisation.

Fig. 1(b) and (c) shows DW position vs. time in a homogeneous nanowire driven by magnetic field $H_z = 300$ Oe and electric current with density $J = 2 \times 10^{12}$ A/m² respectively. DWs showed a constant

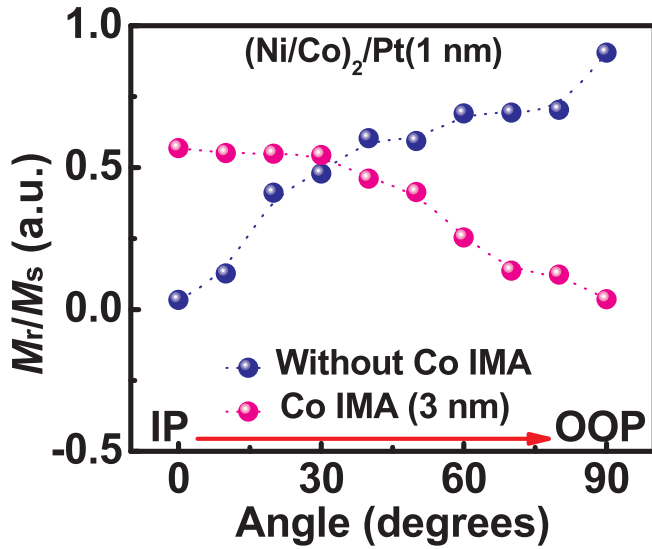


Fig. 4. The normalised remanent magnetisation (M_r/M_s) change with applied field angles.

velocity of 240 m/s and 254 m/s with respect to the magnetic field and electric current. As the next step, we simulated a structure by introducing the region with in-plane magnetisation to achieve tilted magnetisation. The magnetic anisotropy at the magnetisation tilted position will be altered, to $K_{u1} = 5.5 \times 10^5 \text{ J/m}^3$. The magnetisation tilted angle was defined by θ , expressing as $(0, \sin(\frac{\pi}{180}\theta), \cos(\frac{\pi}{180}\theta))$.

Fig. 2(a) shows the nanowire with tilted magnetisation (M). The tilted magnetisation area has the dimensions of 200 nm in length and 144 nm in width. The tilt angle was set to $\theta = 5^\circ$, expressing as $(0, \sin(\frac{\pi}{36}), \cos(\frac{\pi}{36}))$. DW shows steady motion before reaching pinning site. At the position with tilted M , it was pinned. We plotted the DW position as a function of time for different values of the applied magnetic field (H) and electric current (J), as shown in Fig. 2 (b) and (c), where the magnetisation tilt angle is 5° at the pinning position. When the magnetic field is below 840 Oe, DW moves up to and gets pinned at the position with tilted M position, and the velocity is increasing with magnetic field increasing, which is determined from the slope of the steady motion. When the field is increased to 850 Oe, DW was depinned and travelled to the end of the nanowire. A similar trend was observed for current-driven DW motion. The depinning current density was determined to be at $3.64 \times 10^{12} \text{ A/m}^2$. Fig. 2(d) and (e) summarise the depinning field and current for different tilt angles with various damping constant α , from 5° to 25° . The depinning field and current does not consistently increase with tilt angles. For different values of damping constant α , the depinning current is larger for a larger value of α (for a fixed tilt angle). It is to be noted that all the simulations in this study were performed at zero K. In general, the depinning field and depinning current are expected to be lower at higher temperatures, such as the operating temperature of a domain wall device [27].

3. Results and discussion

The simulation results predicted the possibility of DW pinning with tilted magnetisation. To achieve the tilted magnetisation experimentally, we grew Co/Ni multilayers using magnetron sputtering, and the stack structure is shown in Fig. 3(a), which is abbreviated as $(\text{Co/Ni})_2$. Ta (5 nm) is used as the seed layer for good adhesion. The underlayer Pt (5 nm) is used for out-of-plane orientation of $(\text{Co/Ni})_2$. The thickness of Co and Ni layers are 0.25 nm and 0.5 nm respectively. The capping layer Pt was deposited, to protect the magnetic film from oxygenation. In addition, it can also be used to tune the exchange coupling strength with the in-plane orientation layer.

Fig. 3(a1) shows the hysteresis loops for $(\text{Co/Ni})_2$ multilayer measured using vibrating sample magnetometry (VSM) applied field along different directions, as determined by inset in Fig. 3(a1). The loop shows perfect square shape along the out-of-plane (OOP) direction, which is labelled as 90. Along in-plane (IP) direction, labelled as 0, the loop shows a straight line. Both these results indicate that the material has an out-of-plane magnetic anisotropy. While the loops for samples with 3 nm thick Co show the square shape along the IP direction and straight line along OOP direction, which indicate the in-plane magnetisation, as shown in Fig. 3(a2). The inset shows the Co sample stack for measurement.

Fig. 3(b) and (c) show stacks of the PMA with IMA layer, where the spacer layer Pt is 1 nm and 2 nm respectively. By depositing a Pt spacer layer with various thickness, the exchange coupling can be tuned, thus altering to tilt magnetisation of $(\text{Co/Ni})_2$ PMA layer to a different angle. It is important to note that the thickness of the Pt spacer determines the exchange coupling and hence the extent of tilting of magnetisation in the PMA layer. In the thin film level, the thickness of the Pt layer was optimised, and it was observed that the magnetisation of $(\text{Co/Ni})_2$ multilayer could be tilted for a Pt thickness of 1 nm, as shown in Fig. 3 (b1 and b2), where (b2) is the zoom-in figure for (b1). However, when the Pt layer is 2 nm thick, $(\text{Co/Ni})_2$ multilayers and Co layer are decoupled, as shown in Fig. 3(c1 and c2).

We calculated the normalised remanent magnetisation (M_r/M_s) change with applied field angles, as shown in Fig. 4. The value of M_r/M_s for $(\text{Co/Ni})_2$ PMA sample shows the highest along OOP direction and lowest along IP direction, which confirms the excellent PMA properties of $(\text{Co/Ni})_2$ sample. For $(\text{Co/Ni})_2$ PMA coupled with Co IMA sample, the value of M_r/M_s shows highest along IP direction and lowest along OOP direction. It was expected to have a maximum value at some particular angles, where the magnetisation of the PMA layer would tilt. However, the magnetization measured by VSM mostly picked up from Co IMA layer, whose thickness is larger. Hence, the tilt angle could not be measured.

Since it is difficult to estimate the tilt angle at the pinning site experimentally, we calculated the tilt angle by micromagnetic simulations using mumax3 [24]. A cell size of $1 \times 1 \times 1 \text{ nm}^3$ was used in this simulation. The IMA layer's material parameters are: $M_{s1} = 1000 \times 10^3 \text{ A/m}$, $K_{u1} = 200 \times 10^3 \text{ J/m}^3$ and the exchange stiffness, $A_1 = 10 \times 10^{-12} \text{ J/m}$ [28]. The magnetisation of the IMA Co layer lies in the (0, 1, 0) direction and the thickness is 3 nm. The material parameters for the PMA layers are: $M_{s0} = 655 \times 10^3 \text{ A/m}$, $K_{u0} = 374 \times 10^3 \text{ J/m}^3$ and exchange stiffness $A_0 = 15 \times 10^{-12} \text{ J/m}$ [29]. The thickness of the PMA layer is 2 nm. The exchange coupling A_{ex10} between PMA and IMA layers is defined as $A_{ex10} = S \cdot A_{ex-average}$, where S is a scale factor, indicating the coupling strength and $A_{ex-average}$ is the average exchange coupling between PMA and IMA layers. Fig. 5(a–d) show the captured magnetisation images in the y-z plane with various scale factor S . With an increase in S , the tilting of magnetisation of the PMA layer to y-direction was enhanced. When $S = 0.04$, the magnetisation of the PMA layer is fully tilted to the in-plane direction, as shown in Fig. 5(d).

We calculated the magnetisation tilt angle θ at the remanence using the following equation,

$$\theta = \cos^{-1}(m_{rem}/m_{sat})$$

where m_{rem} is the normalised remanence (M_{rem}/M_{sat}), and m_{sat} is the normalised saturation, equal to 1 in this simulation [29]. We simulated the hysteresis loops with different scale factor values. Then we extracted magnetisation of the PMA layer along different directions at remanence state and plotted magnetisation (M) component with scale factor change. The magnetisation along x-direction (m_x) is almost zero. While the magnetisation along y-direction (m_y) increases with an increasing S scale factor, the magnetisation along z-direction (m_z) decreases, as shown in Fig. 6(a). These results indicate that the magnetisation of the PMA layer is tilted to the y-direction with larger

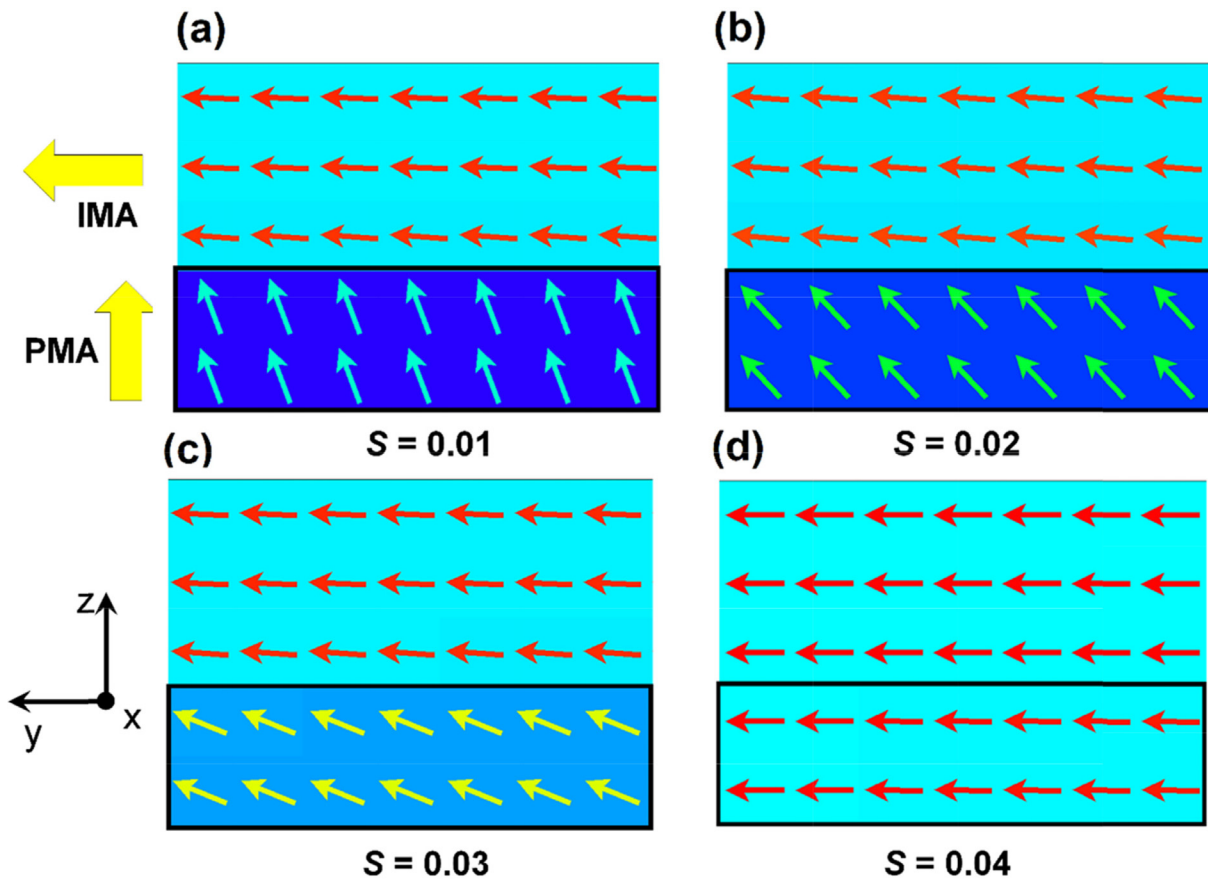


Fig. 5. (a–d) The magnetisation configuration with different exchange coupling strength, which is defined by scale factor S from 0.01 to 0.04. The bottom layer highlighted by the black box is the PMA layer, and the top layer is the IMA layer.

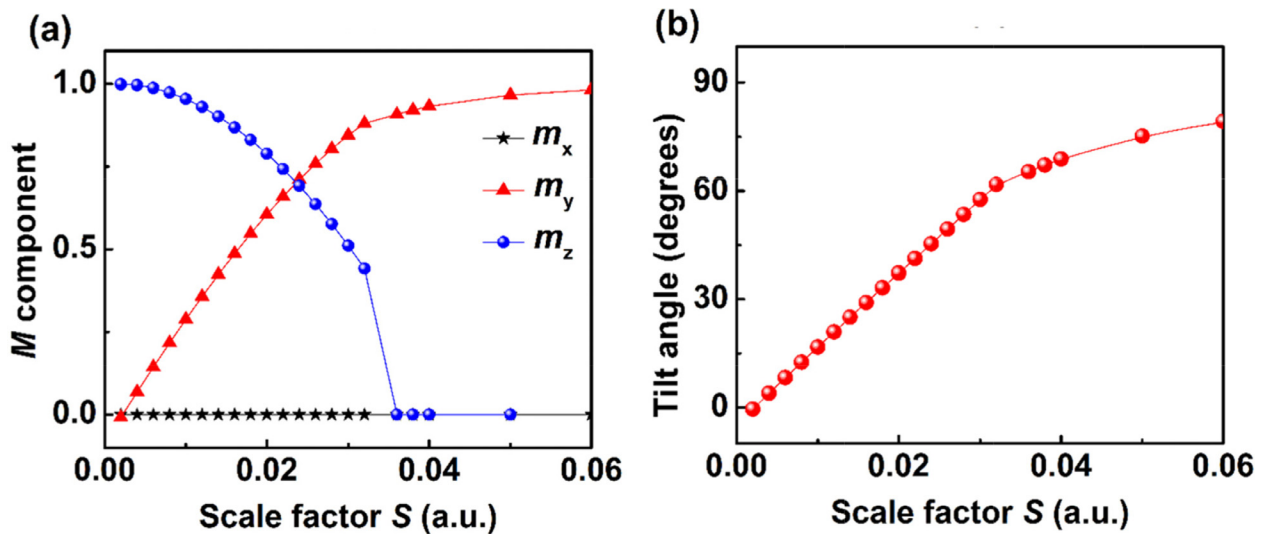


Fig. 6. (a) The magnetisation (M) component and (b) the tilt angle calculated with various exchange coupling A_{ex10} .

exchange coupling. Fig. 6(b) shows the tilt angle with various scale factor S , which increases linearly up to $S = 0.03$ with a tilt angle of 60° .

To test the pinning at the device level, $(\text{Co/Ni})_2$ nanowires with Pt as capping layer were patterned to have a width of $1\ \mu\text{m}$ and length of $100\ \mu\text{m}$, by using electron-beam lithography (EBL) and ion milling etching. One more step of electron beam exposure was carried out to make a resist trench for depositing Co layer. After the Co layer was deposited by sputtering, lift off was performed to strip the resist. These Co crossbars, which are orthogonal to $(\text{Co/Ni})_2$ nanowires, have a

width of $800\ \text{nm}$ and a thickness of $3\ \text{nm}$. A pad was fabricated at the left side of the wires to nucleate domains. The sample was first saturated with a $+5\ \text{kOe}$ field along the OOP direction. Subsequently, a $1\ \text{ms}$ pulsed magnetic field was applied in the reverse direction. To observe the nucleated domains, the MagVision Kerr microscopy system was used. The magnetic field required for nucleating a DW was different for samples with different Pt thickness. For sample with a Pt thickness of $1\ \text{nm}$, the required field was $180\ \text{Oe}$, whereas for sample with $2\ \text{nm}$ thick Pt it was $150\ \text{Oe}$.

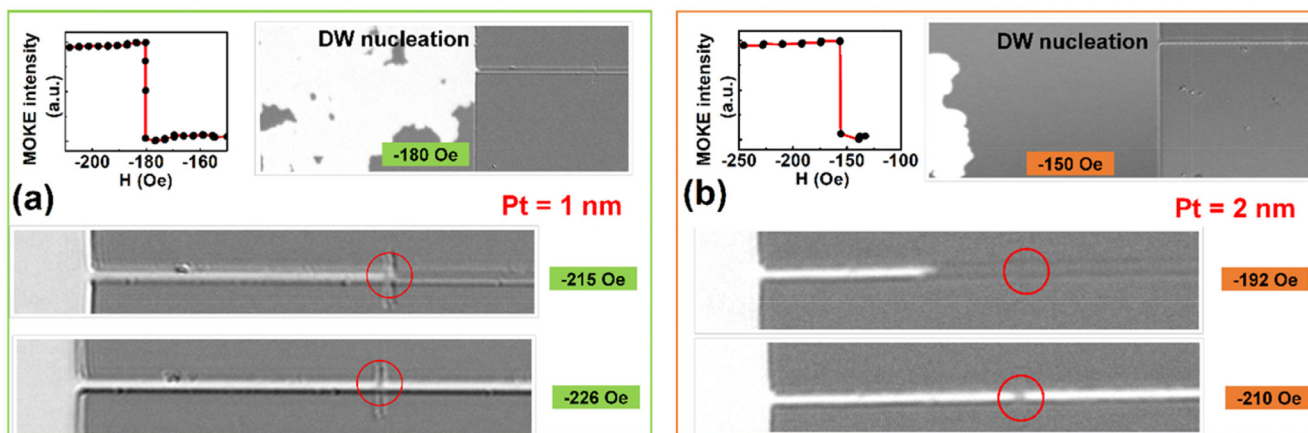


Fig. 7. DW was introduced by applying the pulsed magnetic field. (a) Then DW shows pinning for Pt thickness of 1 nm and (b) no pinning for Pt thickness of 2 nm upon the application of the reverse pulsed magnetic field.

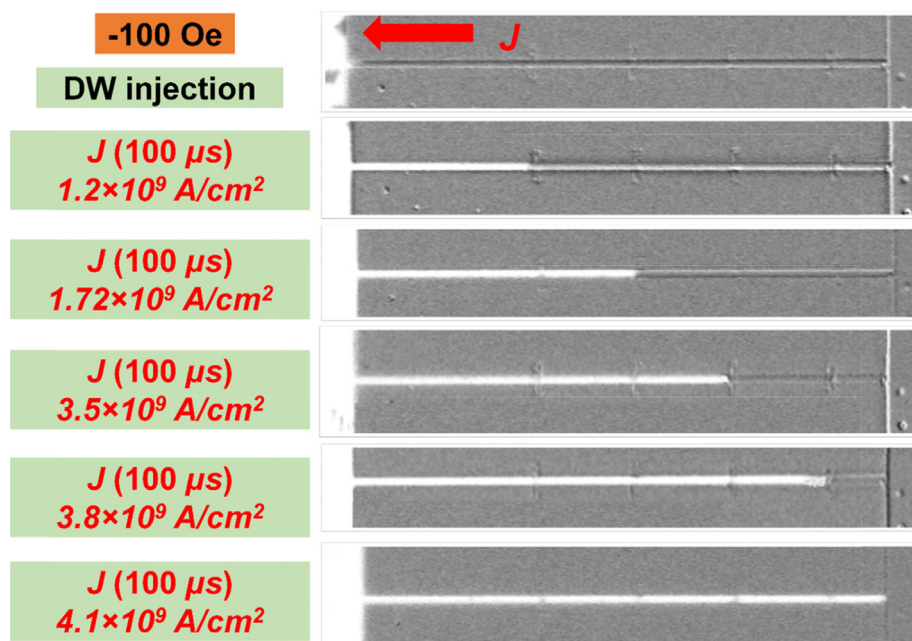


Fig. 8. DW pinning and depinning driven by electric current. The current density was noted at the left side.

After nucleating a reversed domain, the pulsed magnetic field was applied with increasing amplitude while keeping the pulse duration constant. As can be seen in Fig. 7(a), DW can be pinned at a field of -215 Oe in the first position for sample with a Pt thickness of 1 nm. The domain wall gets depinned at a higher applied field ~ -226 Oe. In contrast, when Pt spacer layer thickness is 2 nm (Fig. 7(b)) DW shows continuous motion i.e. DW does not get pinned at the crossbar position. These results indicate that the pinning is effective at an optimum thickness of Pt, where the exchange coupling is optimum.

We also carried out DW pinning investigations, in the device with Pt thickness of 1 nm, by driving the DW using electrical current. In this study, the Co IMA crossbar layer was designed to have different widths such as 1 μm , 800 nm, 600 nm, and 400 nm from the left to right of the device. At first, the device was saturated by applying $+5$ kOe along the OOP direction. Subsequently, a pulsed magnetic field of -100 Oe was applied. After a domain was nucleated at the nucleation pad, the DW was moved towards the nanowire with an external magnetic field. Then, a series of pulse current J was passed through the wire in the direction indicated by the arrow J . The DW was found to move along the electron direction.

Fig. 8 shows the DW position for different current density values, as noted at the left side of Fig. 8. It was observed that the DW can be successfully pinned at the pinning sites and is able to be depinned with an increased current density. This allows the DW to be pinned at the next pinning site with a higher pinning strength.

4. Conclusion

We proposed and showed that the regions with a tilted magnetisation could pin the domain walls in a ferromagnetic nanowire. The simulation results support the possibility for the tilted magnetisation to pin domain walls. In the experimental study, the tilted magnetisation of the $(\text{Co/Ni})_2$ PMA layer can be achieved by depositing a magnetic layer of Co with in-plane magnetic anisotropy. The spacer layer between PMA and IMA layer should be less than 1 nm to tune the exchange interaction strength between them. The angle of the magnetisation of the PMA layer increases linearly with increasing exchange coupling up to 60° , and then begin saturating towards the in-plane direction. The simulation results were confirmed by the study on $(\text{Co/Ni})_2$ devices, where the pinning of domain wall was observed in $(\text{Co/Ni})_2$ wire at the

position of the crossbar driven by electric current, and its propagation was controlled by regions with tilted magnetisation.

Acknowledgements

The authors thank the partial financial support from NTU start-up grant and MOE Tier 1 grant RG163/65. The work was supported by an Industry-IHL Partnership Programs (NRF2015-IIP001-001 and NRF2015-IIP003-001). The supports from a RIE2020 ASTAR AME IAF-ICP Grant (No.I1801E0030) and an ASTAR AME Programmatic Grant (No. A1687b0033) is also acknowledged. WSL and SNP are members of the Singapore Spintronics Consortium (SG-SPIN).

Appendix A. Supplementary data

Supplementary data to this article can be found online at <https://doi.org/10.1016/j.jmmm.2019.165410>.

References

- [1] S.S. Parkin, X. Jiang, C. Kaiser, A. Panchula, K. Roche, M. Samant, Magnetically engineered spintronic sensors and memory, *Proc. IEEE* 91 (2003) 661–680.
- [2] D.A. Allwood, G. Xiong, C.C. Faulkner, D. Atkinson, D. Petit, R.P. Cowburn, Magnetic domain-wall logic, *Science* 309 (2005) 1688–1692.
- [3] Y. Zhang, W. Zhao, J.O. Klein, D. Ravelosona, C. Chappert, Ultra-high density content addressable memory based on current induced domain wall motion in magnetic track, *IEEE Trans. Magn.* 48 (2012) 3219–3222.
- [4] S.S.P. Parkin, M. Hayashi, L. Thomas, Magnetic domain-wall racetrack memory, *Science* 320 (2008) 190–194.
- [5] S. Fukami, M. Yamanouchi, K.J. Kim, T. Suzuki, N. Sakimura, D. Chiba, S. Ikeda, T. Sugibayashi, N. Kasai, T. Ono, H. Ohno, 20-nm magnetic domain wall motion memory with ultralow-power operation, *IEEE Int. Electron Devices Meeting IEEE* 2013 (2013) 3–5.
- [6] S.N. Piramanayagam, K. Srinivasan, Recording media research for future hard disk drives, *J. Magn. Magn. Mater.* 321 (2009) 485–494.
- [7] X.Y. Fong, Y.S. Kim, K. Yogendra, D.L. Fan, A. Sengupta, A. Raghunathan, K. Roy, Spin-transfer torque devices for logic and memory: prospects and perspectives, *IEEE Trans. Comp.-Aided Des. Integr. Circuits Syst.* 35 (2016) 1–22.
- [8] R. Sbiaa, H. Meng, S.N. Piramanayagam, Materials with perpendicular magnetic anisotropy for magnetic random access memory, *Phys. Status Solidi Rapid Res. Lett.* 5 (2011) 413–419.
- [9] R. Sbiaa, S.N. Piramanayagam, Recent developments in spin transfer torque MRAM, *Phys. Status Solidi Rapid Res. Lett.* 11 (2017) 1700163.
- [10] S. Bhatti, R. Sbiaa, A. Hirohata, H. Ohno, S. Fukami, S.N. Piramanayagam, Spintronics based random access memory: a review, *Mater. Today* 20 (2017) 530–548.
- [11] C.T. Boone, J.A. Katine, M. Carey, J.R. Childress, X. Cheng, I.N. Krivorotov, Rapid domain wall motion in permalloy nanowires excited by a spin-polarized current applied perpendicular to the nanowire, *Phys. Rev. Lett.* 104 (2010) 097203.
- [12] D. Chiba, M. Kawaguchi, S. Fukami, N. Ishiwata, K. Shimamura, K. Kobayashi, T. Ono, Electric-field control of magnetic domain-wall velocity in ultrathin cobalt with perpendicular magnetization, *Nat. Commun.* 3 (2012) 888.
- [13] K.J. Kim, Y. Yoshimura, T. Ono, Current-driven magnetic domain wall motion and its real-time detection, *Jpn. J. Appl. Phys.* 56 (2017) 10.
- [14] Z. Meng, S. He, J. Qiu, T. Zhou, G. Han, K.-L. Teo, Domain wall motion in ultrathin $\text{Co}_{70}\text{Fe}_{30}/\text{Pd}$ multilayer nanowires with perpendicular anisotropy, *J. Appl. Phys.* 119 (2016) 083905.
- [15] S.H. Yang, K.S. Ryu, S. Parkin, Domain-wall velocities of up to 750 m s⁻¹ driven by exchange-coupling torque in synthetic antiferromagnets, *Nat. Nanotechnol.* 10 (2015) 221–226.
- [16] G.S.D. Beach, C. Nistor, C. Knutson, M. Tsoi, J.L. Erskine, Dynamics of field-driven domain-wall propagation in ferromagnetic nanowires, *Nat. Mater* 4 (2005) 741–744.
- [17] Y. Gao, B. You, H.L. Yang, Q.F. Zhan, Z. Li, N. Lei, W.S. Zhao, J. Wu, H.Q. Tu, J. Wang, L.J. Wei, W. Zhang, Y.B. Xu, J. Du, Stochastic domain wall depinning in permalloy nanowires with various types of notches, *AIP Adv.* 6 (2016) 125124.
- [18] A. Himeno, K. Kondo, H. Tanigawa, S. Kasai, T. Ono, Domain wall ratchet effect in a magnetic wire with asymmetric notches, *J. Appl. Phys.* 103 (2008) 07E703.
- [19] Y. Gao, B. You, X.Z. Ruan, M.Y. Liu, H.L. Yang, Q.F. Zhan, Z. Li, N. Lei, W.S. Zhao, D.F. Pan, J.G. Wan, J. Wu, H.Q. Tu, J. Wang, W. Zhang, Y.B. Xu, J. Du, Depinning of domain walls in permalloy nanowires with asymmetric notches, *Sci. Rep.* 6 (2016) 32617.
- [20] S.H. Huang, C.H. Lai, Domain-wall depinning by controlling its configuration at notch, *Appl. Phys. Lett.* 95 (2009) 032505.
- [21] V. Mohanan, P.S.A. Kumar, Chirality dependent pinning and depinning of magnetic vortex domain walls at nano-constrictions, *J. Magn. Magn. Mater.* 422 (2017) 419–424.
- [22] T.L. Jin, F.N. Tan, W.C. Law, W.L. Gan, I. Soldatov, R. Schafer, C. Ma, X.X. Liu, W.S. Lew, S.N. Piramanayagam, Nanoscale modification of magnetic properties for effective domain wall pinning, *J. Magn. Magn. Mater.* 475 (2019) 70–75.
- [23] T.L. Jin, D. Kumar, W.L. Gan, M. Ranjbar, F.L. Luo, R. Sbiaa, X.X. Liu, W.S. Lew, S.N. Piramanayagam, Nanoscale compositional modification in co/pd multilayers for controllable domain wall pinning in racetrack memory, *Phys. Status Solidi RRL* 12 (2018) 1800197.
- [24] A. Vansteenkiste, J. Leliaert, M. Dvornik, M. Helsen, F. Garcia-Sanchez, B. Van Waeyenberge, The design and verification of MuMax3, *AIP Adv.* 4 (2014) 107133.
- [25] Y. Zhang, W. Zhao, J.O. Klein, C. Chappert, D. Ravelosona, Peristaltic perpendicular-magnetic-anisotropy racetrack memory based on chiral domain wall motions, *J. Phys. D: Appl. Phys.* 48 (2015) 105001.
- [26] S. Zhang, Z. Li, Roles of nonequilibrium conduction electrons on the magnetization dynamics of ferromagnets, *Phys. Rev. Lett.* 93 (2004) 127204.
- [27] E. Martinez, L. Lopez-Diaz, L. Torres, C. Tristan, O. Alejos, Thermal effects in domain wall motion: micromagnetic simulations and analytical model, *Phys. Rev. B* 751 (2007) 174409.
- [28] M.A. Bahri, R. Sbiaa, Geometrically pinned magnetic domain wall for multi-bit per cell storage memory, *Sci. Rep.* 6 (2016) 28590.
- [29] S. Chung, S.M. Mohseni, V. Fallahi, T.N.A. Nguyen, N. Benatmane, R.K. Dumas, J. Åkerman, Tunable spin configuration in Co/Ni-NiFe spring magnets, *J. Phys. D: Appl. Phys* 46 (2013) 125004.